Hindawi Publishing Corporation
International Journal of Photoenergy
Volume 2013, Article ID 687693, 8 pages
http://dx.doi.org/10.1155/2013/687693

Research Article

Photovoltaic High-Frequency Pulse Charger for Lead-Acid Battery under Maximum Power Point Tracking

Hung-I. Hsieh,[1] Sheng-Fang Shih,[1] Jen-Hao Hsieh,[2] and Chi-Hao Wang[2]

[1] *Department of Electrical Engineering, National Chiayi University, Chiayi 60004, Taiwan*
[2] *Department of Electrical Engineering, Chung Yuan Christian University, Chungli 320, Taiwan*

Correspondence should be addressed to Hung-I. Hsieh; hihsieh@mail.ncyu.edu.tw

Received 30 November 2012; Accepted 30 May 2013

Academic Editor: Keith Emery

A photovoltaic pulse charger (PV-PC) using high-frequency pulse train for charging lead-acid battery (LAB) is proposed not only to explore the charging behavior with maximum power point tracking (MPPT) but also to delay sulfating crystallization on the electrode pores of the LAB to prolong the battery life, which is achieved due to a brief pulse break between adjacent pulses that refreshes the discharging of LAB. Maximum energy transfer between the PV module and a boost current converter (BCC) is modeled to maximize the charging energy for LAB under different solar insolation. A duty control, guided by a power-increment-aided incremental-conductance MPPT (PI-INC MPPT), is implemented to the BCC that operates at maximum power point (MPP) against the random insolation. A 250 W PV-PC system for charging a four-in-series LAB (48 V_{dc}) is examined. The charging behavior of the PV-PC system in comparison with that of CC-CV charger is studied. Four scenarios of charging statuses of PV-BC system under different solar insolation changes are investigated and compared with that using INC MPPT.

1. Introduction

Renewable energy sources have become indispensable and applicable in our life in consideration to the lack of fossil fuel, especially for the photovoltaic and wind energies. As for energy storage, lead-acid battery (LAB) is always the interesting device due to low cost; even its lifecycle time is low. Fortunately, the experiment reported that, after charging the battery in 5–10 hours with a short-period large current, the sulfating crystallization covered on the plates of positive electrode area will be reduced, and the battery is without overheat and thereby increases the discharge efficiency to extend battery life [1–3]. Thus, the pulse charge method has become one of the available charging strategies in battery management. The LAB is basically composed of two electrodes, the negative electrode made of metallic lead (Pb) and the positive one lead-oxide (PbO_2), immersed in a sulphuric acid solution (H_2SO_4), which produces chemical reaction during charging and discharging processes. During discharge state, both the electrodes in battery will build up lead sulfate $PbSO_4$ and the electrolyte is then converted to H_2O, but the opposite process will occur in charging state. When the battery approaches 85–95% of the state of charge (SOC), the majority of the $PbSO_4$ will be converted to Pb and PbO_2, in which the battery voltage might be greater than the gassing voltage. The overcharge reaction possibly results in the gas evolution of hydrogen appearing at negative electrode and of oxygen at positive electrode. This undesired phenomenon may lead to heat, increasing charging time, and shorten the battery life, even exists explosive potential if the gas is not vented. Above all, if some $PbSO_4$ is crystallized on the pores of positive electrode, the discharging current will be limited due to the reduction of effective surface area on the positive electrode. In order to prolong the battery life, a high-frequency photovoltaic pulse charger (PV-PC) system for LAB is presented, which contributes the pulsate effect for delaying the mentioned sulfating crystallization during the adjacent tiny pulse break times. In this work, a boost current converter (BCC) associated with the PV module is modeled to maximize the energy charging to LAB under maximum power transfer [4]. In order to maximize the energy pumped from PV module, a duty cycle control guided by a power-increment-aided

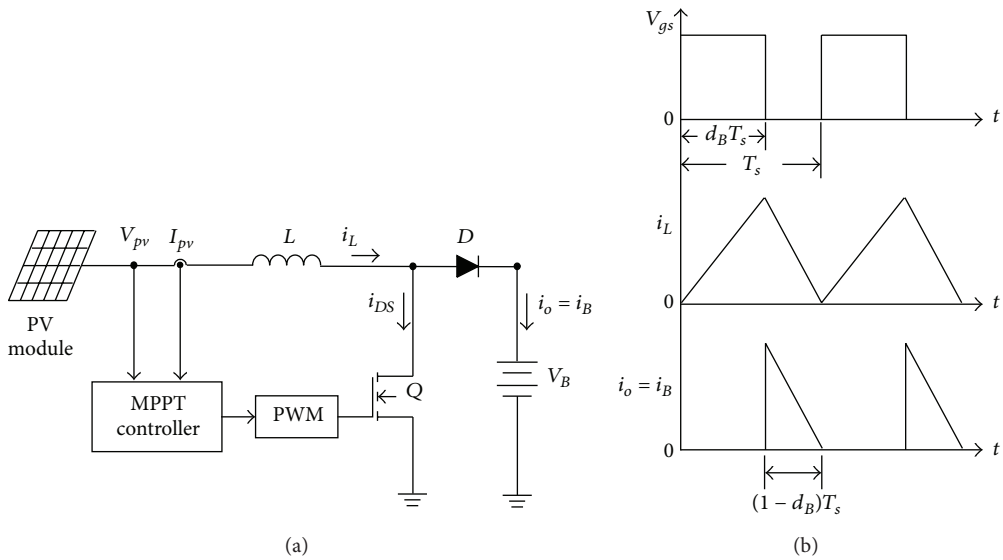

FIGURE 1: (a) Proposed PV-PC system and (b) predicted energy-pumped waveforms of PV-BCC at boundary mode.

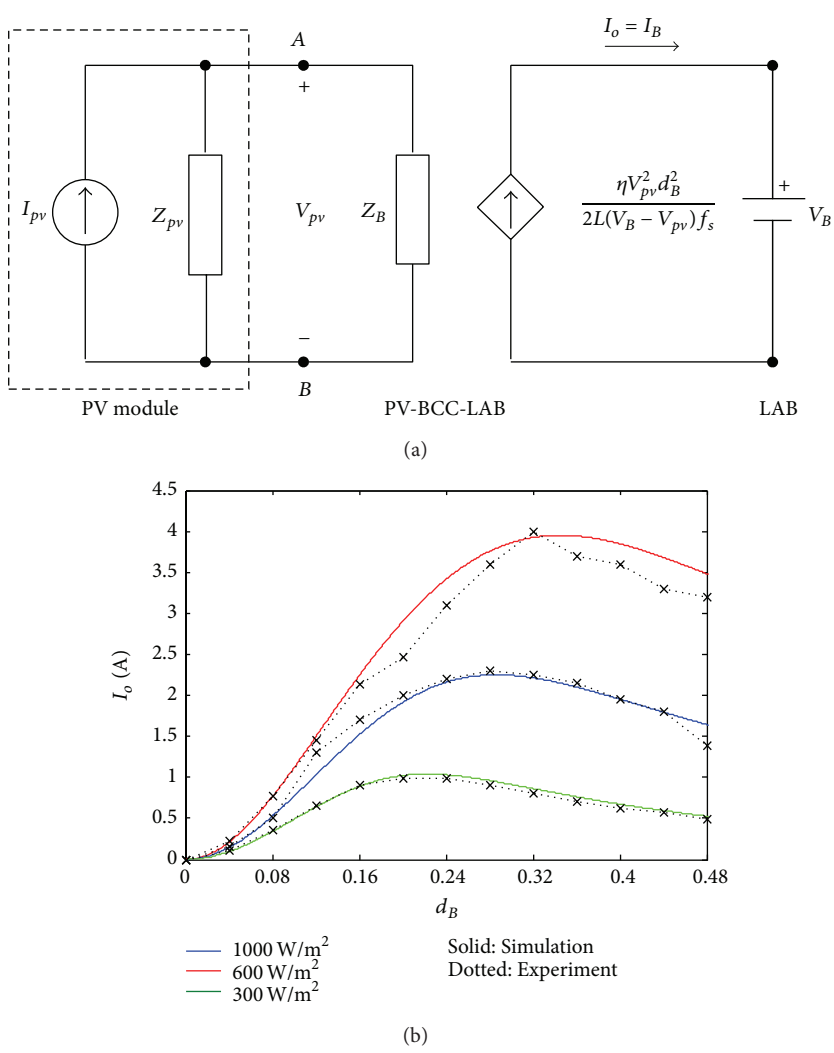

FIGURE 2: (a) The model of the proposed PV-PC and (b) simulated and experimented output-to-control responses.

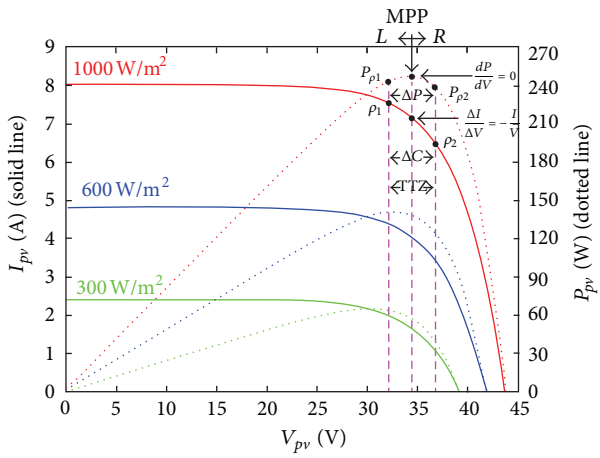

FIGURE 3: I_{pv}-V_{pv} and P_{pv}-V_{pv} characteristic curves for a two-in-series PV module, where a tracking threshold zone (TTZ) is indicated for distinguishing PI-coarse tracking zone and INC-fine tracking zone [6].

incremental-conductance maximum power point tracking (PI-INC MPPT), derived from the incremental-conductance maximum power point tracking (INC MPPT), is adopted to sustain the PV-BCC pumping energy from PV module that is fast and accurate against the random solar insolation [4–8]. The weakness of the INC-MPPT is its ambiguous incremental conductance occurring in the left side of the MPP, which may delay the tracking behavior of MPPT. To clearly describe the dynamic tracking behavior in charging, four scenarios of solar insolation change under the guidance of PI-INC MPPT and INC-MPPT are, respectively, investigated and compared to each other in this work. An experimental study for verifying the charging behavior of the PV-PC system with a four-in-series 45-AH (ampere hour) LABs (48 V_{dc}) is examined. The charging characteristics of the PV-PC system in comparison with that of conventional constant-current constant-voltage (CC-CV) charger are studied. Experimental result validates that high-frequency pulse train can actually delay the sulfating crystallization on the plates of electrodes of the LAB, which prolongs the battery life.

2. Analysis of PV-PC System

Figure 1(a) shows the circuit diagram of the PV-PC system, which is formed by a BCC guided by a MPPT controller. Dynamic states of the BCC at boundary condition are shown in Figure 1(b), in which the output current i_o is certainly a form of pulse train that is used as a charging source. The PV BCC driven by a duty period $d_B T_s$ from PI-INC MPPT can operate between discontinuous-conduction mode (DCM) and boundary-conduction mode (BCM) for pulse charging to the LAB.

For convenience in analysis, the steady state of PV-BCC in BCM is described. If a battery V_B greater than maximum V_{pv} is adopted and all components are presumed to be ideal, the peak inductor current $i_{L,pk}$ of the PV-BCC in BCM from Figure 1(b) can be represented by

$$i_{L,pk} = \frac{V_{pv}}{L} \cdot d_B T_s, \tag{1}$$

where L is the boost inductor, d_B the duty ratio, and T_s the switching period. We then have average PV current I_{pv}:

$$I_{pv} = \frac{V_B V_{pv}}{V_B - V_{pv}} \cdot \frac{d_B^2}{2Lf_s}, \tag{2}$$

where switching frequency $f_s = 1/T_s$. If power efficiency η is considered, the average output current I_o $(= I_B)$ to LAB from (2) will be

$$I_o = \frac{\eta V_{pv}^2 d_B^2}{2L\left(V_B - V_{pv}\right) f_s}. \tag{3}$$

Equation (3) represents the control-to-output transfer function, in which the output current I_o is proportional to square of duty ratio d_B and inversely proportional to switching frequency f_s. The model and simulation of control-to-output transfer function are presented in Figures 2(a) and 2(b), respectively. The duty ratio d_B of PV-BCC is designed associated with the PV characteristic as shown in Figure 3. The output power of PV-BCC can be obtained by

$$P_o = \frac{\eta V_B V_{pv}^2 d_B^2}{2L\left(V_B - V_{pv}\right) f_s}. \tag{4}$$

If an interleaved configuration is considered in the PV-BCC, the average output current I_o and power P_o can be easily obtained from (3) and (4) by multiplying two.

3. PI-INC MPPT for PV-PC System

The PV-BCC guided by PI-INC MPPT controller can draw energy from PV module fast and accurate according to the guidance specified on I_{pv}-V_{pv} and P_{pv}-V_{pv} characteristic curves in Figure 3, in which the tracking references for executing power-increment tracking (PI) and incremental-conductance (INC) tracking are clearly described in [6, 8]. The PI-INC MPPT can provide a PI-coarse tracking quick toward a specified threshold-tracking zone (TTZ) using P_{pv}-V_{pv} curve, to avoid delay tracking that stems from some ambiguous conductance detection in the right-hand side of maximum power point (MPP) in I_{pv}-V_{pv} curve by using INC MPPT method [4, 5, 9]. In Figure 3, two mutual equivalent TTZs are, respectively, defined in the I_{pv}-V_{pv} and P_{pv}-V_{pv} curves used to distinguish the roles of PI-INC MPPT tracking and conventional INC MPPT. A PI-coarse tracking along P_{pv}-V_{pv} curve executes quick toward TTZ when the PV-BCC operates outside the TTZ. Once the detected power increment ΔP is within TTZ, INC-fine tracking is provided toward the MPP using I_{pv}-V_{pv} curve. Thus, a fast and accurate tracking performance is applicable in PI-INC MPPT in comparison to that in the conventional INC-MPPT. The MPP

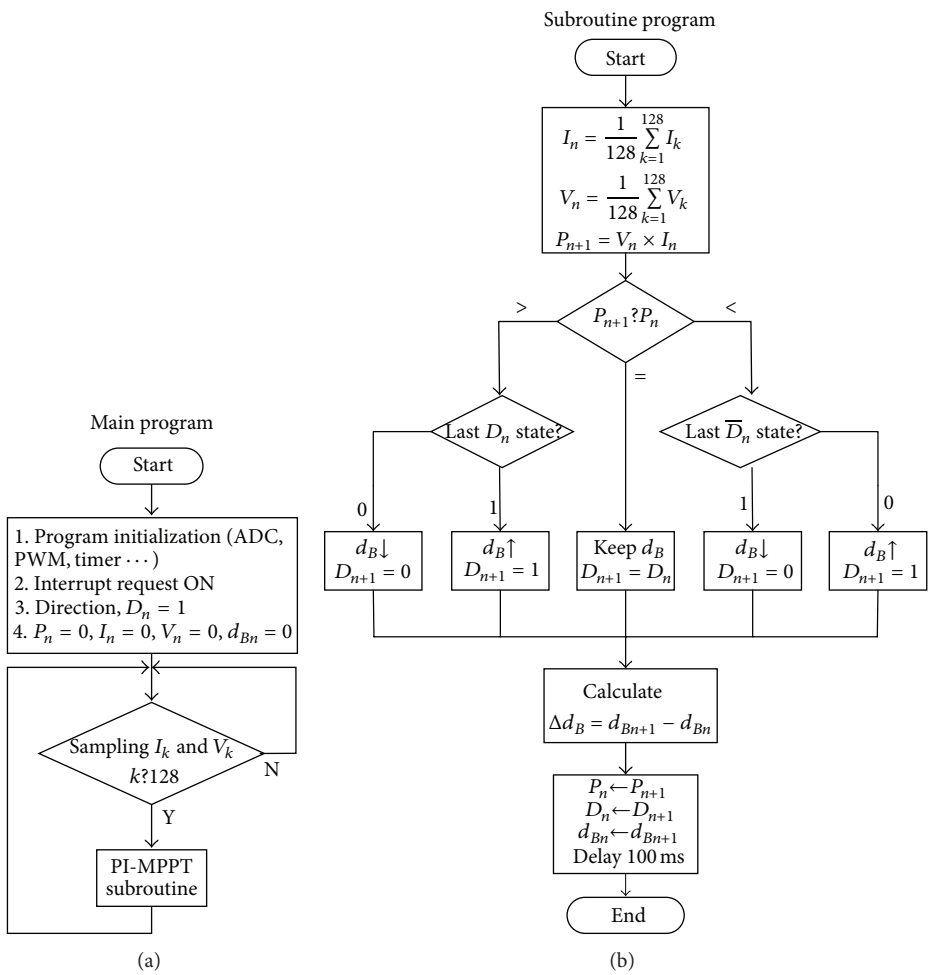

Figure 4: Programming of PI-INC MPPT: (a) main program and (b) subroutine program without THZ, as a simplified case of PI-INC MPPT.

for INC MPPT, reported by Wasynczuk [5], can then be given by

$$\frac{dI_{pv}}{dV_{pv}} = -\frac{I_{pv}}{V_{pv}}, \qquad \frac{\Delta I_{pv}}{\Delta V_{pv}} \approx \frac{dI_{pv}}{dV_{pv}} = -\frac{I_{pv}}{V_{pv}}. \tag{5}$$

It is clearly shown that in Figure 3 the measure ΔC is bounded by the two ratios ρ_1 and ρ_2 on the I_{pv}-V_{pv} curve, and correspondingly the measure ΔP is bounded between limits $P_{\rho 1}$ and $P_{\rho 2}$ on the P_{pv}-V_{pv} curve, in which $P_{\rho 1}$ and $P_{\rho 2}$ are derived from the two ratios ρ_1 and ρ_2. From the specified ΔC on the I_{pv}-V_{pv} curve, the tracking bound in TTZ will be

$$-\rho_1 \frac{I_{pv}}{V_{pv}} > \Delta C > -\rho_2 \frac{I_{pv}}{V_{pv}} \tag{6}$$

and outside the TTZ when

$$\Delta C > -\rho_1 \frac{I_{pv}}{V_{pv}} \tag{7}$$

or

$$\Delta C < -\rho_2 \frac{I_{pv}}{V_{pv}}, \tag{8}$$

where ΔC is defined as

$$\Delta C = \frac{\Delta I_{pv}}{\Delta V_{pv}}. \tag{9}$$

The two ratios ρ_1 and ρ_2 are real numbers. Equation (9) is always negative because ΔI_{pv} and ΔV_{pv} have opposite signs. Accordingly, the corresponding relation to PI-INC MPPT derived from the specified bounds of INC MPPT will be, from (6)–(9),

$$P_{\rho 1} > \Delta P > P_{\rho 2} \tag{10}$$

within TTZ, where $\Delta P = P_{n+1} - P_n$, $\Delta V = V_{n+1} - V_n$, and $\Delta I = I_{n+1} - I_n$, and

$$\Delta P > P_{\rho 1} \tag{11}$$

or

$$\Delta P < P_{\rho 2} \tag{12}$$

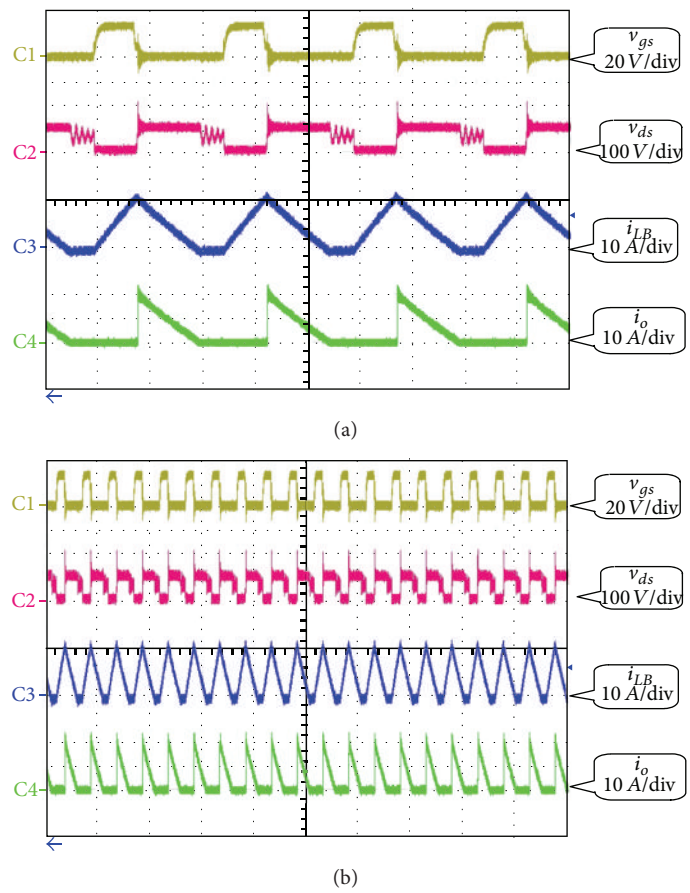

Figure 5: Measured waveforms of PV-BCC at 600 W/m^2, MPPT conditions: $V_{pv} = 32.7$ V, $I_{pv} = 4.3025$ A, $f_s = 40$ kHz, and $d_B = 0.29$, (a) Hor.: 10 μ/div. and (b) Hor.: 50 μ/div.

outside of TTZ. The two power threshold limits in (10) are defined by

$$P_{\rho 1} \equiv (1 - \rho_1)\,\Delta V I_{n+1},$$
$$P_{\rho 2} \equiv (1 - \rho_2)\,\Delta V I_{n+1}. \tag{13}$$

The flow chart of PI-INC MPPT for duty control presented in Figure 4 will enable MPPT controller adaptively providing proper duty ratio d_B for PV-BCC to pump energy from PV module at MPP in which a simplified program with $P_{\rho 1} = P_{\rho 2} = 0$ is examined. In other words, the program is a special case of the PI-INC MPPT without TTZ.

Table 1: Comparison of MPPT tracking scenarios under different insolation changes.

Scenario	Insolation jump step (W/m^2)	Initial jump location	PI-INC MPPT (sec)	INC MPPT (sec)
1	0 → 600	L	9	33
2	600 → 1000	R	6	13
3	1000 → 300	L	15	142
4	300 → 1000	R	22	32

L: Left-hand side of the MPP.
R: Right-hand side of the MPP.

4. Design and Realization

A 250 W PV-PC system configured as in Figure 1(a) consisting of a two-in-series PV module (Kyocera KC130T), a BCC, and a four-in-series LAB (Kawasaki MF50B24, 12 V$_{dc}$, 45 AH, each) is designed and realized for assessing the charging behavior of LAB guided by PI-INC MPPT, and validating the feasibility in application. The PV-PC system operates at constant frequency of 40 kHz with duty varied from 0 to 0.36 under solar insolation from 0 to 1 kW/m^2, in which the duty at $d_B = 0.36$ is when solar insolation at 1 kW/m^2, where the peak charging current for LAB is 16 A. The program of PI-INC MPPT is executed by microchip dsPIC33FJ06GS202 according to the tracking guidance in Figure 4, in which a simplified case of PI-INC MPPT without THZ is presented for instance. The PI-coarse tracking along P_{pv}-V_{pv} curve can perform fast and accurate tracking toward MPP in comparison with the INC tracking along I_{pv}-V_{pv} curve. The waveforms of the PV-BCC working at solar insolation of 600 W/m^2 and 1000 W/m^2 are measured in Figures 5 and 6, respectively, in which the boost inductor current i_L is in DCM

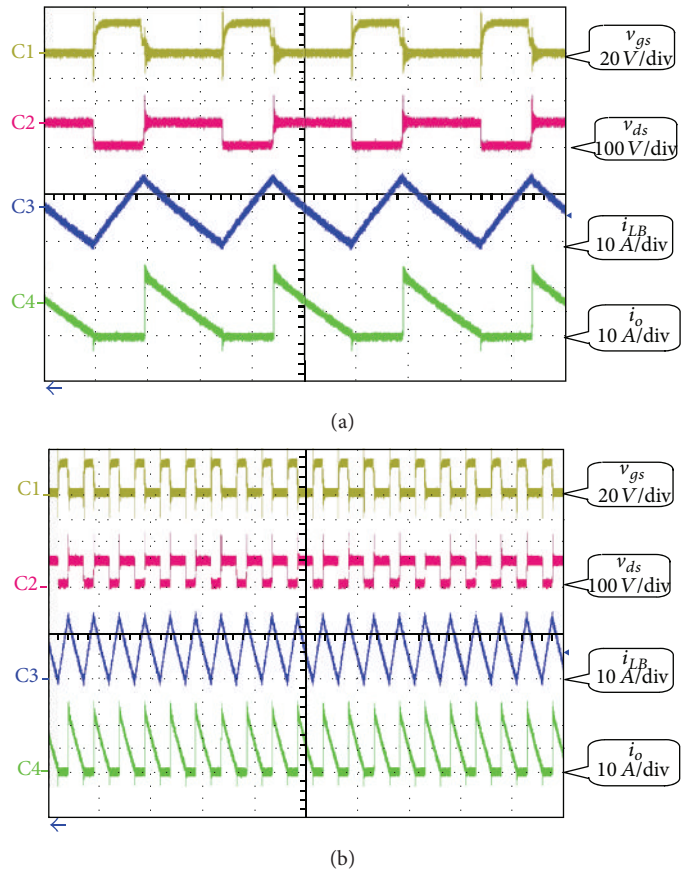

Figure 6: Measured waveforms of PV-BCC at 1000 W/m^2, MPPT conditions: V_{pv} = 34.3 V, I_{pv} = 47.193 A, f_s = 40 kHz, and d_B = 0.36, (a) Hor.: 10 μ/div. and (b) Hor.: 50 μ/div.

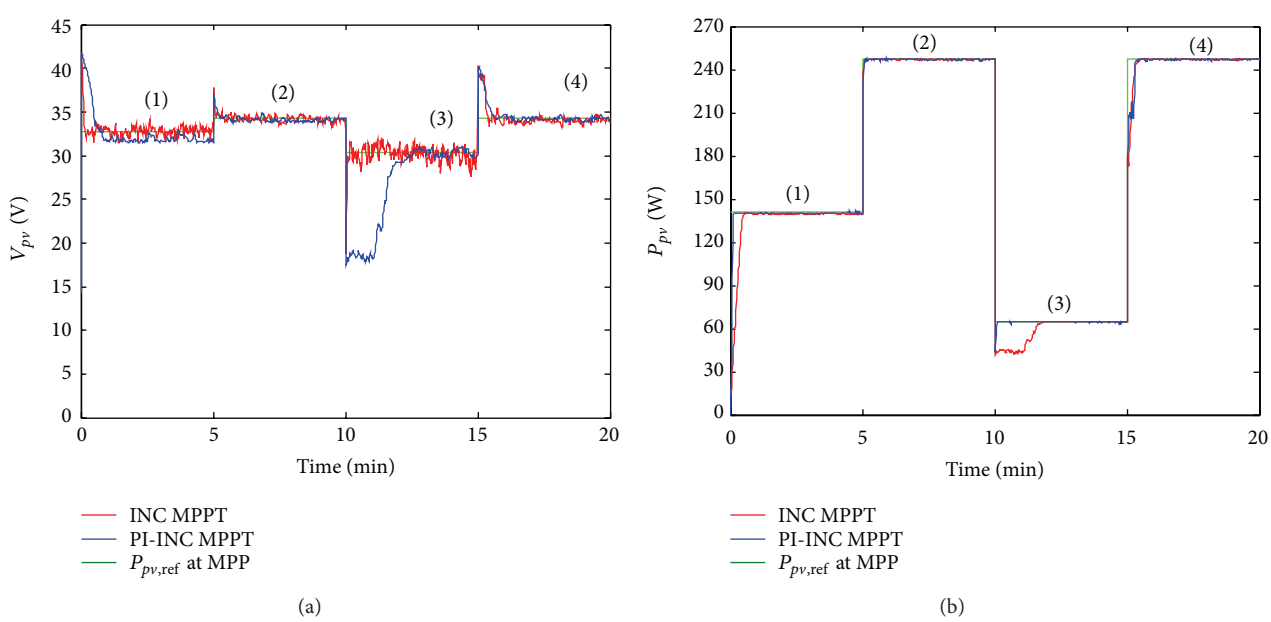

Figure 7: Tracking comparison of PI-INC MPPT and INC MPPT for PV-PC system under four scenarios of solar insolation change (a) voltage tracking behavior and (b) power tracking behavior.

Table 2: Comparison of charging statuses between CC-CV and pulse charge.

SOC (%)	CC-CV Voltage (V)	CC-CV Capacity (%)	PV pulse charge Voltage (V)	PV pulse charge Capacity (%)	Charging time (min.)
30	48.73	30	48.73	30	0
35	49.32	43.84	49.42	46.19	15
40	49.51	48.30	49.57	49.71	30
45	49.69	52.53	49.76	54.17	45
50	49.88	56.99	49.9	57.45	60
55	50	59.80	50.01	60.04	75
60	50.17	63.79	50.2	64.49	90
65	50.32	67.31	50.36	68.25	105
70	50.48	71.06	50.53	72.24	120
75	50.63	74.58	50.68	75.76	135
80	50.8	78.57	50.88	80.45	150
85	50.96	82.33	51.06	84.68	165
90	51.12	86.08	51.25	89.13	180
95	51.27	89.60	51.43	93.36	195
	51.43	93.36			210

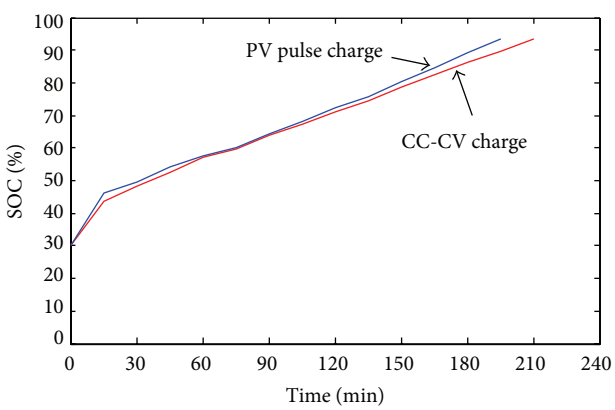

Figure 8: Comparison of charging behaviors between CC-CV and PV-PC.

at 600 W/m^2 but in CCM at 1000 W/m^2. In spite of the state modes either DCM or CCM, the output currents i_o clearly shown in Figures 5(b) and 6(b) are always available pulse trains for charging the LABs. Figure 7 shows the comparison of the tracking behaviors of PI-INC MPPT and INC MPPT in the PV-PC system under four kinds of solar insolation scenarios. The voltage tracking in Figure 7(a) and power tracking in Figure 7(b) clearly display that the PI-INC MPPT is much more fast and accurate toward the MPP than the INC MPPT. The PI-INC MPPT can only pay few seconds to track at MPP when the solar jump step initially occurs in either side of the MPP. In other words, there is no ambiguous detection happened in PI-INC MPPT. As for the INC MPPT, it is ambiguous to detect the incremental conductance in the left-hand side of the MPP, which may lead much delay in MPPT, such behaviors as in scenarios 1 and 3; the tracking times toward MPP should be much more over 4–10 times of the PI-INC MPPT. The measured data of tracking response shown in Table 1 show that the PI-INC MPPT is more reliable than INC MPPT in tracking process during the four scenario changes; in particularly, there is no abrupt delay response occurring in PI-INC MPPT during the insolation change, in comparison to the response of INC MPPT. The state of charge (SOC) of the PV-PC system compared with that of CC-CV charger is shown in Figure 8, and the detail charging statuses are measured in Table 2. The measured result reveals faster response of 195 min for PV-PC system than that of 210 min for CC-CV charger over about 8%, compared at SOC about 95%.

5. Conclusion

The PV pulse charge directly using PV energy without through a dc-to-dc converter as energy buffer enhances the utilization of renewable energy. The brief pulse break existing between adjacent high-frequency pulses can actually perform the discharge refreshing of LAB for delaying sulfate crystallization on electrodes. The charging behavior using pulse charge is faster than that using CC-CV charge, which reveals that the resulted sulfate crystallization on the positive electrode of the LAB is slow in pulse charging process, which is good for prolonging the battery life. Moreover, the PI-INC MPPT compared with INC MPPT advantages much better tracking behavior without abrupt tracking delay during solar insolation change.

Acknowledgments

The authors would like to thank the National Science Council with the project NSC 101-2221-E-415-010 and joint project of Lien-Chang Electronics Enterprise Ltd. Co. 991206 for their financial support.

References

[1] L. T. Lam, H. Ozgun, O. V. Lim et al., "Pulsed-current charging of lead/acid batteries-a possible means for overcoming premature capacity loss?" *Journal of Power Sources*, vol. 53, no. 2, pp. 215–228, 1995.

[2] J. J. A. Wilkinson and G. A. Covic, "A new pulse charging methodology for lead acid batteries," *IPENZ Transactions*, vol. 25, no. 1, pp. 1–16, 1998.

[3] S. Minami, Y. Onishi, S. J. Hou, and A. Kozawa, "A new intense pulse-charging method for the prolongation of life in lead-acid batteries," *Journal Asian Electric Vehicles*, vol. 2, no. 1, pp. 541–544, 2004.

[4] R. L. Mueller, M. T. Wallace, and P. Iles, "Scaling nominal solar cell impedances for array design," in *Proceedings of the 1st World Conference on Photovoltaic Energy Conversion (WCPEC '94)*, pp. 2034–2037, December 1994.

[5] O. Wasynczuk, "Dynamic behavior of a class of photovoltaic power system," *IEEE Transactions on Power Apparatus and Systems*, vol. 102, no. 9, pp. 3031–3037, 1983.

[6] G. C. Hsieh, C. Y. Tsai, and H. I. Hsieh, "Photovoltaic power-increment-aided incremental-conductance maximum power

point tracking using variable frequency and duty controls," in *Proceedings of the IEEE 3rd International Symposium on Power Electronics for Distributed Generation Systems (PEDG '12)*, pp. 542–549, Aalborg, Denmark, 2012.

[7] H. I. Hsieh, S. F. Shih, J. H. Hsieh, and G. C. Hsieh, "A study of high-frequency photovoltaic pulse charger for lead-acid battery guided by PI-INC MPPTin," in *Proceedings of the International Conference on Renewable Energy Research and Applications (ICRERA '12)*, pp. 283–288, Nagasaki, Japan, November 2012.

[8] G. C. Hsieh, H. I. Hsieh, C. Y. Tsai, and C. H. Wang, "Photovoltaic power-increment-aided incremental-conductance MPPT with two-phased tracking," *IEEE Transactions on Power Electronics*, vol. 28, no. 6, pp. 2895–22911, 2013.

[9] K. H. Hussein, I. Muta, T. Hoshino, and M. Osakada, "Maximum photovoltaic power tracking: an algorithm for rapidly changing atmospheric conditions," *IEE Proceedings*, vol. 142, no. 1, pp. 59–64, 1995.